Journal of the Meteorological Society of Japan, Vol. 75, No. 3, pp. 701–715, 1997

Multiresolution Fourier Transform and Its Application to Analysis of CO_2 Fluctuations over Alert

By Jian-Ping Huang, Kaz Higuchi and Neil B. A. Trivett

Carbon Cycle Research Laboratory, Atmospheric Environment Service
Downsview, Ontario, Canada

(Manuscript received 30 September 1996, in revised form 10 March 1997)

Abstract

Difficulties in using conventional Fourier spectral analysis to explore the temporal variation of CO_2 short-term fluctuations have indicated the need for some new statistical techniques. It is suggested here that the Multiresolution Fourier Transform (MFT) can be used for interpreting such fluctuations. The technique is adapted from wavelet theory in signal processing. To demonstrate the usefulness of this technique, some examples of analytic fluctuation are first examined. The examples suggest that this technique might be useful for analysis of fluctuations that exhibit locality in both frequency and time.

MFT is then applied to study the CO_2 fluctuations measured at Alert from 1988 to 1995. The results show that the CO_2 concentration over Alert has two dominant regimes of quasi-periodic short-term fluctuation: 1)20–50 day intraseasonal fluctuation and 2) 6–14 day synoptic fluctuation. Both the amplitude and frequency of these fluctuations are strongly modulated by the seasonal cycle and the largest amplitude appears during winter time. In addition, these short-term fluctuations have significant interannual variability, especially for the synoptic fluctuation.

1. Introduction

Time series of atmospheric CO_2 measurements made at a number of monitoring stations in the Northern Hemisphere show many interesting features (Higuchi and Daggupaty, 1985; Higuchi *et al.*, 1987; Trivett *et al.*, 1989; Higuchi *et al.*, 1995; Lejenäs and Holmén, 1996; Engardt *et al.*, 1996). Proper interpretations of these features are important in obtaining an increased understanding of the processes governing the spatial and temporal distributions of carbon among the major carbon reservoirs (atmosphere, ocean, and terrestrial biosphere). Some of the most notable characteristics of a CO_2 time series are: (1) an upward secular trend, reflecting an increasing carbon content in the atmosphere produced mainly by fossil fuel combustion; (2) a seasonal cycle produced mainly by the photosynthetic-decay process of the terrestrial biosphere; (3) short-term fluctuations superimposed on the seasonal cycle, reflecting the regional and local sources and sinks and (4) interannual variability in all of the above three features. Among the problems not yet well understood are the temporal structure of short-term fluctuations and how the seasonal cycle modulates them. The CO_2 gas is a passive and nonreactive chemical species with a relatively long residence time in the atmosphere. Since an air parcel coming in contact with a local or regional source/sink of CO_2 will retain, barring any substantial mixing, the flux characteristics of the CO_2 source/sink, better understanding of the short-term fluctuations observed in atmospheric CO_2 measurements is very important in addressing the issue of local sources and sinks in the global carbon cycle.

Recent observational studies indicate that, although a consistent CO_2 efflux from the forest tundra of North Russian occurs throughout the year, the locations of maximum CO_2 efflux do exhibit seasonality (Zimov *et al.*, 1996). Winter CO_2 efflux is a major component of annual CO_2 flux in boreal Russia and, in general, could contribute to the high atmospheric CO_2 concentration observed in winter in the far north. If this phenomenon is widespread, it suggests that the large seasonal amplitude of atmospheric CO_2 at high latitude is due more to a substantial CO_2 efflux in winter rather than to high biospheric productivity in summer. The present paper attempts to study the temporal structure of short-term fluctuations of atmospheric CO_2 over Alert. Alert is a Canadian CO_2 monitoring station located on the northern tip of Ellesmere Island in the Canadian Arctic Archipelago .

Due to the variety of periodic or nonperiodic deterministic and some undeterministic sources and sinks, time series of atmospheric CO_2 are not stationary in time. It has been pointed out by Huang and North (1996) that traditional methods related to Fourier spectral decomposition are inappropriate in an analysis of non-stationary time series. Fourier spectral analysis can identify the underlying frequencies and their relative contributions to the time series, but it shows no explicit information regarding their temporal locality. Therefore, non-stationary signals which appear only during short time intervals are poorly detected by Fourier analysis, since these signals are averaged out over the entire data record. In searching for a fundamental structure in the time-frequency domain, even very weak signals may be important if they influence the overall response of the system. In this regard, further understanding of CO_2 fluctuations demands special efforts in time series analysis.

Efforts have been made to overcome the drawback of Fourier analysis by constructing a "window" in the time domain so that local spectral information can be identified. Gabor (1946) first introduced a Gaussian window with predefined width. With a fixed window width, however, the so-called Windowed Fourier Transform (WFT) is not suitable for detecting a signal that possesses a wide range of time scales. This was a major motivation for studying the wavelet transform in mathematics and in applied areas, *e.g.*, Grossmann and Morlet (1984). Wavelet transform relates window width to the frequency of base function (wavelet), forming a flexible time window to overcome the WFT's weakness. Considerable attention has been given to applying the wavelet technique to the study of atmospheric and oceanographic phenomena, (Gambis, 1992; Gamage and Blumen 1993; Hudgins *et al.*, 1993 Meyers *et al.* 1993; Foufoula-Georgiou and Kumar, 1994; Weng and Lau 1994; Gollmer *et al.* 1995; Lau and Weng 1995; Mak, 1995; Hudgins and Huang, 1996).

However, the wavelet transform is displayed in the state space. Although the spectral information can be surmised from the state space representation, the frequency is not explicitly presented. Furthermore, a serious problem arises when the window width is connected with frequency. Once the window widens, local information will be diluted on a broader base and time locality is degenerated. When a signal involves components that vary in wide ranges of time and frequency, a more flexible base is desirable. Wilson *et al.* (1992) have recently proposed a generalized wavelet transform called *Multiresolution Fourier Transform (MFT)* to meet this need. The MFT combines the windowed Fourier Transform and the wavelet transform into a single transform. It has some particular advantages for studying climate signals. The motivation of this paper is to introduce this newly-developed approach to study the various fluctuations that occur in time series of continuous atmospheric CO_2 measurements obtained at Alert, Canada from 1988 to 1995. By using MFT, we can obtain spectral information related to the temporal variation of the relative contributions made to the CO_2 variability at Alert by various spectral terms with certain characteristic frequencies. This eventually allows us to speculate on the identity of various processes which possess these frequencies.

Before we get into the actual spectral analysis of the Alert continuous CO_2 measurements by the MFT, we first briefly introduce the wavelet transform and multiresolution Fourier transform in Sections 2 and 3. Then we illustrate some MFT applications on analytic climate fluctuations in Section 4. Section 5 presents the MFT analysis of CO_2 fluctuations over Alert. Finally, we summarize our main results in Section 6.

2. Fourier Transforms and Wavelet Transforms

In this section we first briefly review some basic properties of Fourier, windowed Fourier and wavelet transforms. In the next section we introduce the central concept of *multiresolution Fourier transform,* which will be used for our analysis. A comprehensive treatment of the wavelet subject can be found in Combes *et al.* (1989), Chui (1992), Daubechies (1992), and references therein. Further details regarding multiresolution Fourier transform may be found in Wilson *et al.* (1992).

The theory described in this and the subsequent sections is developed within the context of *any* separable Hilbert space, such that the operator $\int() \cdot dt$ is a linear functional satisfying Reisz's Theorem. In the discrete case the measures are also discrete, so that the integrals may be equivalently written as convergent summations, which *in itself* does not introduce any numerical errors. However, sampling the time-series amounts to quantizing and mapping onto a finite-dimensional Hilbert space (*i.e.*, digitizing and truncating the record), which produces quantization errors, windowing, and anti-aliasing effects. Such important considerations belong to the discipline of signal processing, and will not be discussed here.

2.1 Fourier transform

The Fourier transform (FT) is one of the most commonly used tools to study the frequency spectrum of a time series. Given a time series $x(t)$, the standard Fourier transform can be written as

$$F(f) = \int_{-\infty}^{+\infty} x(t) e^{-i2\pi ft} dt. \tag{1}$$

where f is the frequency and t is the time. Fourier spectrum analysis generally provides frequency information about the energy content of measured, and presumed stationary, time-series data. Characteristic properties of time series such as total energy and dominant or average frequency can be readily derived from the estimated spectrum. However, the Fourier transform produces a fixed frequency spectrum from the entire signal and therefore can not explicitly provide any *local* information regarding the time evolution of its spectral characteristics. Furthermore, the representation of a temporally localized signal using the FT is very inefficient and requires a large number of Fourier components. In an extreme case where a signal is represented by a delta function in time, the signal would be represented by an infinite number of components in FT representation. Moreover, if the time series is reversed in time, the new time series will have exactly the same FT representation, even though the local information of the two time series might be completely different.

2.2 Windowed Fourier transform

The study of non-stationary time series by localizing signals in both frequency and time domains was first introduced by Gabor (1946) using windowed Fourier transform (WFT; also known as the Short Time Fourier Transforms). The windowed Fourier transform centered at τ is given by:

$$\Gamma(f,\tau) = \int_{-\infty}^{+\infty} x(t)g(t-\tau)e^{-i2\pi ft}dt \qquad (2)$$

where $g(t)$ is the window function, given by

$$g(t) = \frac{1}{\sigma\sqrt{2\pi}}e^{-\frac{t^2}{2\sigma^2}} \qquad (3)$$

with width determined by the standard deviation σ of the Gaussian. τ is the translation parameter with the same dimension as t. For any τ, the windowed Fourier transform $\Gamma(f,\tau)$ provides the spectrum of a windowed segment of $x(t)$, centered at time τ. In WFT, a time series is examined over a fixed time-frequency window at constant sub-intervals in the time and frequency domains. When a wide frequency range is involved, the fixed time window of the WFT tends to contain a large number of high-frequency cycles and a few low-frequency cycles, or parts of cycles. This often results in an over-representation of the high-frequency components and under-representation of the low-frequency components. Because of the constant frequency increment, the WFT does not have adequate resolution in the very low frequency band; much of the computation effort of the transfer is spent on high frequency components, which results in a large number of spurious spectral peaks. The recently developed wavelet transform addresses the problem of resolution by introducing a flexible window, which narrows while focusing on high-frequency signals and widens while searching the low-frequency background.

2.3 Wavelet transforms

The wavelet transform decomposes a function or a signal into various scales by expanding it in terms of simple functions called *wavelets*. The wavelet transform of a function $x(t)$ is defined as

$$W(\tau,s) = \int_{-\infty}^{+\infty} x(t)\psi_s\left(t-\tau\right)dt,$$

where τ is the translation parameter, s is the dilation parameter, and the function

$$\psi_s(t) = \frac{1}{\sqrt{|s|}}\psi\left(\frac{t}{s}\right) \qquad (4)$$

is called a wavelet. Changing the value of s has the effect of dilating or contracting the function $\psi_s(t)$ and changing τ has the effect of analyzing the $x(t)$ around the point τ. The wavelets $\psi_s(t)$ are then used as "mathematical microscopes", in which ψ characterizes the optics, while t is the position analyzed and $1/s$ the magnification.

For a suitable choice of $\psi_s(t)$, the wavelet transform may also be regarded as a local Fourier transform; for a given position τ, the amplitude of $W(\tau,s)$ will be largest when the scale number s is roughly equal to the local wavenumber of the signal. The choice of the wavelet $\psi(t)$ is neither unique nor arbitrary. The function $\psi_s(t)$ is chosen so that it has a compact support, or has a sufficiently fast decay, to obtain localization in space.

The wavelet transform $W(\tau,s)$ is displayed in the state space defined by the dilation s and the translation τ. Although the spectral information can be surmised from the state space representation, the frequency is not explicitly presented. In any case, there is considerable latitude in the choice of fundamental wavelet $\psi_s(t,s)$. The functional dependence of the fundamental wavelet on the dilation parameter s may also be arbitrarily defined. Extraction of spectral information from a state space representation is possible only for the very simplest of wavelet. The multiresolution Fourier transform can overcome these shortcomings of the wavelet transform.

3. Multiresolution Fourier Transform

Recently, Wilson *et al.* (1992) has proposed a generalized wavelet transform for Fourier analysis: *i.e.*, Multiresolution Fourier Transform (MFT).

3.1 Continuous MFT

For a continuous 1-d time series $x(t)$, its continuous MFT at position τ, frequency f, and scale σ is defined by

$$S(f,\tau,\sigma) = \int_{-\infty}^{+\infty} x(t)g(t-\tau,\sigma)e^{-i2\pi ft}dt \qquad (5)$$

where $g(t,\sigma)$ is an appropriate window function. The windowed Fourier transform $\Gamma(f,\tau)$ is a particular case of $S(f,\tau,\sigma)$ with σ held constant. The primary purpose of the dilation (or scaling) parameter σ is to increase the 'width' of the window function $g(t,\sigma)$ for lower frequencies and vice versa, and is controlled by selecting a specific functional dependency of σ with the frequency f.

Following Stockwell *et al.* (1994), we have used the Gaussian window as window function and chosen the window width to be proportional to the period of the cosinusoid being localized,

$$\sigma = T = \frac{1}{f} \tag{6}$$

where T is the period. Therefore (3) can be rewritten as

$$g(f,t) = \frac{|f|}{\sqrt{2\pi}} e^{-\frac{t^2 f^2}{2}}. \tag{7}$$

The multiresolution Fourier transform is then rewritten as

$$S(f,\tau) = \int_{-\infty}^{+\infty} x(t) \frac{|f|}{2\pi} e^{-\frac{(t-\tau)^2 f^2}{2}} e^{-i2\pi f t} dt \tag{8}$$

or equivalently in terms of their corresponding Fourier transforms

$$S(f,\tau) = \int_{-\infty}^{+\infty} F(\alpha + f) e^{-\frac{2\pi^2 \alpha^2}{f^2}} e^{i2\pi\alpha\tau} d\alpha. \tag{9}$$

The discrete analog of (9) is used to calculate the discrete MFT by taking advantage of the efficiency of the FFT (Fast Fourier Transform) and the convolution theorem.

In essence, this transform takes a one-dimensional function of time into a two-dimensional function of time and frequency. $S(f,\tau)$ is a complex function with amplitude and phase defined by

$$A(f,\tau) = |S(f,\tau)| \tag{10}$$

$$\Phi(f,\tau) = tan^{-1} \frac{Im(S(f,\tau))}{Re(S(f,\tau))}. \tag{11}$$

In analogy with Fourier power spectrum, we can readily define the Multiresolution Fourier Spectrum as

$$P(f,\tau) = S(f,\tau) S^{\star}(f,\tau) = |S(f,\tau)|^2, \tag{12}$$

where an asterisk superscript indicates the complex conjugate.

3.2 The Fourier transform and the inverse of MFT

If the MFT is indeed a representation of the local spectrum, one would expect a straightforward operation of averaging the local spectrum to give the Fourier, or time-averaged spectrum. This is indeed the case, as the integral over all τ gives the Fourier spectrum. Using (9) we have

$$\int_{-\infty}^{+\infty} S(f,\tau) d\tau = \int_{-\infty}^{+\infty} \int_{-\infty}^{+\infty} F(\alpha + f) e^{-\frac{2\pi^2 \alpha^2}{f^2}} e^{i2\pi\alpha\tau} d\alpha d\tau. \tag{13}$$

Rearranging the order of integration (which is possible $\forall$ f $\neq 0$) in order to perform the integration over τ, we have

$$\int_{-\infty}^{+\infty} S(f,\tau) d\tau = \int_{-\infty}^{+\infty} F(\alpha + f) e^{-\frac{2\pi^2 \alpha^2}{f^2}} d\alpha \int_{-\infty}^{+\infty} e^{i2\pi\alpha\tau} d\tau, \tag{14}$$

where the integral over τ can be calculated using the Fourier integral theorem:

$$\int_{-\infty}^{+\infty} e^{i2\pi\alpha\tau} d\tau = \delta(\alpha). \tag{15}$$

Using the delta function $\delta(\alpha)$, the integration over α gives

$$\int_{-\infty}^{+\infty} S(f,\tau) d\tau = F(f), f \neq 0, \tag{16}$$

where $F(f)$ is the Fourier transform of $x(t)$ as defined in (1). For $f = 0$, the MFT is defined such that

$$\int_{-\infty}^{+\infty} S(0,\tau) d\tau = F(0), f = 0. \tag{17}$$

Equations (16) and (17) is striking in the sense that there is a direct relationship between the standard Fourier and multiresolution Fourier transform. One can compute, exactly, the Fourier transform $F(f)$ from $S(f,\tau)$. It follows that $x(t)$ is recoverable, exactly, from $S(f,\tau)$, *i.e.*,

$$x(t) = \int_{-\infty}^{+\infty} \{ \int_{-\infty}^{+\infty} S(f,\tau) d\tau \} e^{i2\pi f t} df. \tag{18}$$

3.3 Discrete MFT

Let $x(k\Delta t)$, $k = 0, 1 \ldots\ldots, N-1$ denote a discrete time series, corresponding to $x(t)$, with a time sampling interval of Δt. Using (9), the MFT component at position τ_k, and frequency f_n can be written for discrete time series as

$$S(f_n,\tau_k) = \sum_{m=0}^{N-1} F(\alpha_m + f_n) e^{-\frac{2\pi^2 \alpha_m^2}{f_n^2}} e^{i2\pi\alpha_m\tau_k}, \tag{19}$$

where $\alpha_m = m/N\Delta t$ is the frequency at scale m, $f_n = n/N\Delta t$ is the frequency at scale n, τ_k is the kth sample point for the original sequence, and $F(f_n)$ is the discrete Fourier transform given by

$$F(f_n) = \frac{1}{N}\sum_{k=0}^{N-1} x(k\Delta t)e^{-i2\pi f_n k}. \quad (20)$$

The discrete inverse of the MFT is

$$x(k\Delta t) = \frac{1}{N}\sum_{n=0}^{N-1}\{\sum_{l=0}^{N-1} S(f_n,\tau_l)\}e^{i2\pi f_n k}. \quad (21)$$

In the limit as $n \to 0$, the width of the Gaussian decreases to zero. The zero frequency is the average of the time series and is constant; that is, the value of $S(f_n,\tau_l)$ for $n = 0$ is simply the average of $x(k\Delta t)$. In the representation (21), the Gaussian function at $n = 0$ is replaced with the Delta function $\delta_{m,0}$ so that MFT is exactly invertible.

4. Analytic Climate Fluctuations

Climatic fluctuations are determined by complex nonlinear interactions between internal dynamics and slowly changing external forcing. The finite-amplitude oscillation in atmosphere is one of the simplest examples. Since Pedlosky (1970) proposed the dual-time-scale concept for nonlinear oscillations, a one-dimensional oscillation is generally depicted as

$$V = A(\tau)\cos(\omega t), \quad (22)$$

where ω is the frequency ($\omega = 2\pi f$), and A is an amplitude that varies on a slow time scale. Many papers have been published since then to determine $A(\tau)$ from different dynamical models, especially from finite-amplitude wave models. However, little has been done to obtain $A(\tau)$ from real or simulated data. This is due to the common use of the Fourier transform to estimate the spectrum from data. In the following, we illustrate the MFT for four modulated fluctuations typical of those commonly encountered in the climate system. The equations are modified from those used by Lau and Weng (1995).

4.1 Amplitude modulation

The amplitude modulated fluctuation is often found in the climate system involving nonlinear interaction between different scales or interference of a frequency component from its sidebands. The fluctuation examined here (Fig. 1a) is a combination of two amplitude modulated fluctuations, which is given by

$$x(t) = A(t)\{\cos(2\pi f_1 t) + \cos(2\pi f_2 t)\}, \quad (23)$$

where

$$A(t) = A_0\cos(2\pi f_m t). \quad (24)$$

Eq. (23) represents a time series or signal with two fundamental oscillation frequencies, *i.e.* $f_1 = 0.1$ and $f_2 = 0.3$, whose amplitude is modulated with the low frequency $f_m = 0.05$. Fig. 1b shows the spectrum of MFT. It can be seen that the two modulated fluctuations are separated in the frequency domain. Both dominant frequencies appear as horizontal lines centered at frequency 0.1 and 0.3, reflecting the constancy of the fundamental periodicity in time. The periodic waveform in time domain corresponds to amplitude modulation. However, the corresponding Fourier spectrum (Fig. 1c) shows two distinct peaks around the corresponding dominant frequencies ($f_1 = 0.1$ and $f_2 = 0.3$).

4.2 Frequency jump

The fundamental frequency of amplitude modulated fluctuation may also jump at some time. This may be found in the occurrence of a catastrophic event. This kind of fluctuation can be defined as

$$x(t) = \begin{cases} A(t)\cos(2\pi f_1 t), t \le 150; \\ A(t)\cos(2\pi f_2 t), t > 150 \end{cases}, \quad (25)$$

where f_1 and f_2 are same as in Eq. (23). Equation (25) shows an abrupt shift in the appearance of the fluctuation near $t = 150$ in the original time series (Fig. 2a). Its MFT (Fig. 2b) is represented by a shift of frequency from $f = 0.1$ to $f = 0.3$. The abruptness of the change is well represented by MFT in the neighborhood of $t = 150$. The corresponding Fourier spectrum (Fig. 2c) shows two distinct peaks at the corresponding frequencies but contains no information on the time of occurrence of the abrupt change. Moreover, comparing Fig. 1 with Fig. 2, it can be seen that while the two time series are completely different, they have similar Fourier spectral representations.

4.3 Frequency modulation

The frequency-modulated fluctuation may be important if the fundamental physical properties of the climate system undergo secular changes such as an increase in atmospheric moisture due to global warming. This may change the stability of the atmosphere and alter the frequency of its normal modes. The analytic fluctuation studied here is a combination of two cosine functions whose frequencies f_1 and f_2 are modulated by changes in phase, and is given by (Fig. 3a)

$$x(t) = A_0\{\cos(2\pi f_1 t + \Phi(t)) + \cos(2\pi f_2 t + \Phi(t))\}, \quad (26)$$

where

$$\Phi(t) = \alpha\sin(2\pi f_m t) \quad (27)$$

and f_1, f_2 and f_m have the same values as in Eq. (23). Eq. (27) shows that the frequency of the cosine varies with time in a period of $T = 1/f_m$. The periodic variation of frequency with time shows up clearly in the spectra of MFT (Fig. 3b). Fig. 3b also shows the effectiveness of the MFT in localized

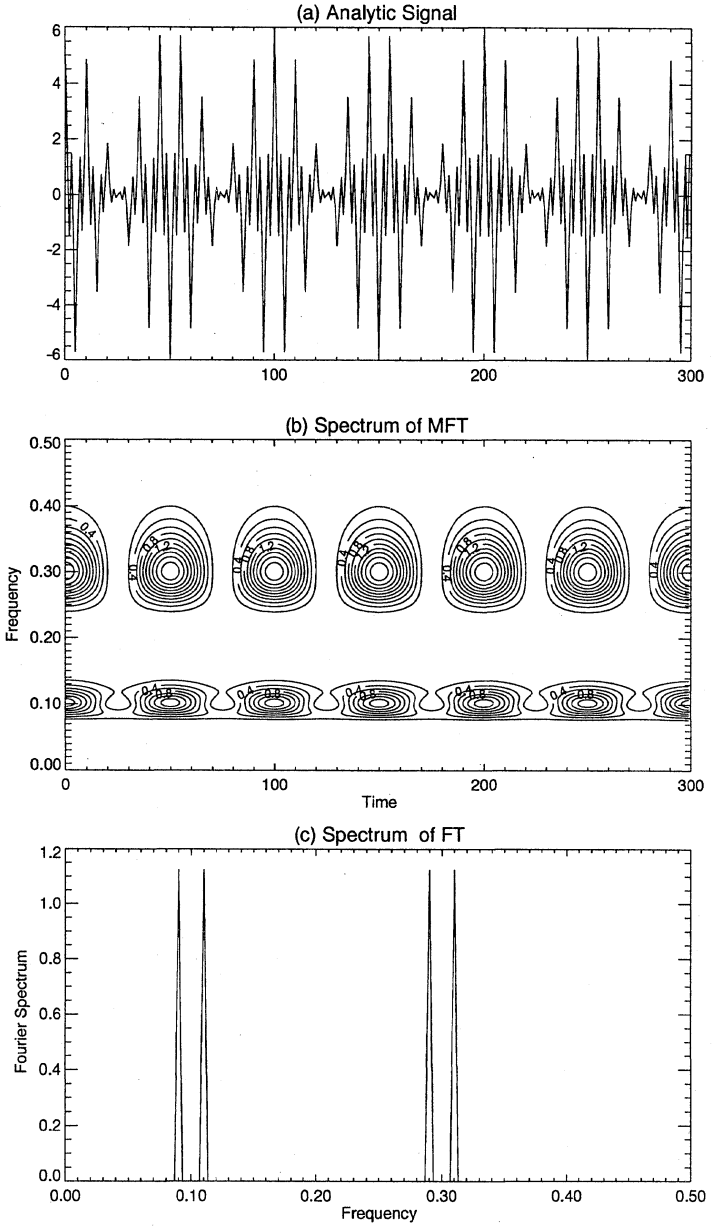

Fig. 1. MFT and FT analysis of an amplitude-modulated fluctuation: (a) time series; (b) spectrum of MFT (the contour interval is 0.2); (c) spectrum of FT.

decomposition into the different frequency components. Since the frequencies evolve constantly and any given single frequency does not exist for a finite time, the Fourier spectrum of this time series (Fig. 3c) shows several peaks.

4.4 Frequency jump within modulation

The final illustrated example shows a frequency jump in a frequency modulated fluctuation. The time series can be written as (Fig. 4a),

$$x(t) = \begin{cases} A_0 \cos(2\pi f_1 t + \Phi(t)), t \leq 150; \\ A_0 \cos(2\pi f_2 t + \Phi(t)), t > 150 \end{cases} \quad (28)$$

where f_1 and f_2 are same as in Eq. (23). Eq. (28) shows an abrupt frequency shift in appearance of the fluctuation near $t = 150$ in the original time series (Fig. 4a). The spectrum of MFT (Fig. 4b) shows that the frequency jump in a frequency modulated fluctuation is well represented by MFT in the neighborhood of $t = 150$. The corresponding Fourier spectrum in Fig. 4c, however, is similar to that in Fig. 3c, even though the local information of the two time series is completely different.

5. Analysis of CO_2 Fluctuation

The multiresolution Fourier transform approach described in Section 3 is now applied to analyses of CO_2 continuous measurements from the Canadian CO_2 monitoring station Alert. Alert is located on

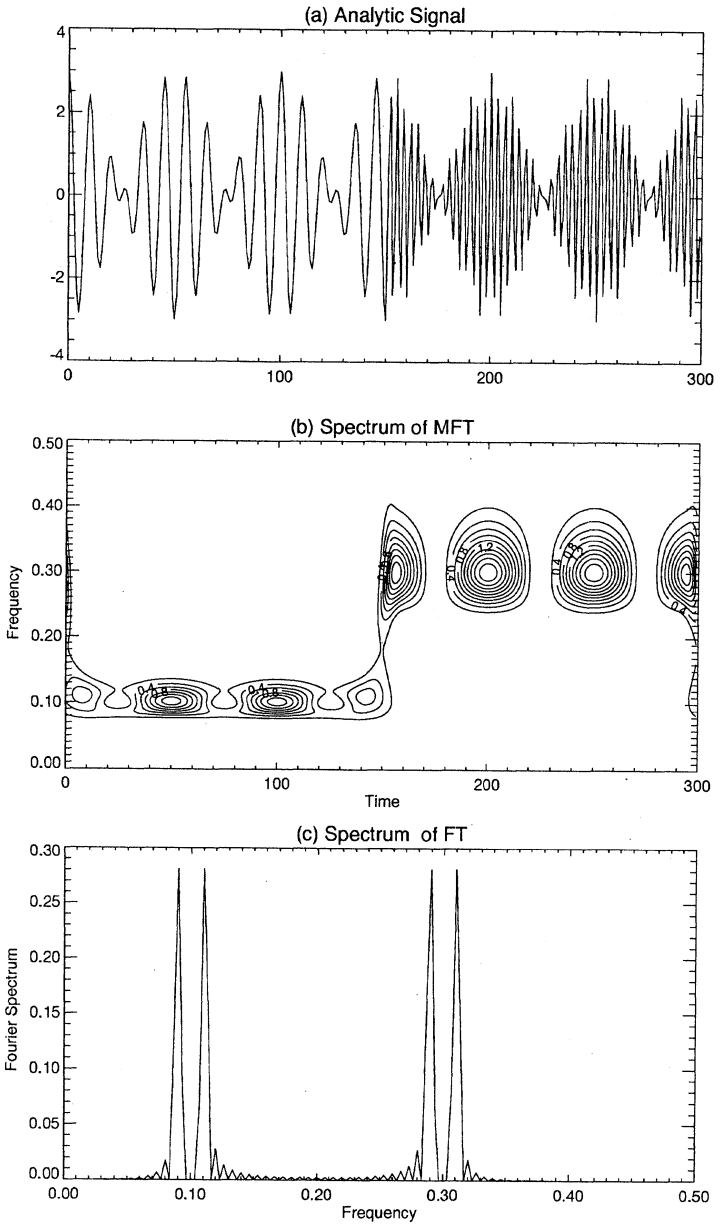

Fig. 2. MFT and FT analysis of an amplitude-modulated fluctuation associated with a frequency jump: (a) time series; (b) spectrum of MFT (the contour interval is 0.2); (c) spectrum of FT.

the northern tip of Ellesmere Island in the Canadian Arctic Archipelago. More than seven years (1 Jan., 1988–31 March, 1995) of daily mean atmospheric CO_2 measurements from Alert are chosen and analyzed. The following steps are applied to this data set to obtain data appropriate for MFT analysis:

(1) The missing data gaps are filled by linear interpolation.

(2) A third-degree polynomial is fitted to the CO_2 time series in a least-square sense to remove the underlying trend (dashed line in Fig. 5a). A secular trend from 1988 to 1995 suggests an average growth rate of around 1.1 ppmv/year.

(3) The detrended time series of CO_2 is then used to construct a composite average seasonal cycle by linearly averaging the seven annual cycles from 1988 to 1994. However, because of the shortness of the data sample, the resulting composite average still retains some fluctuations and fails to produce a smooth seasonal curve. To rectify this, a 30-day low-pass filter is applied to filter out short-term fluctuations. The resulting smooth seasonal cycle (dashed line in Fig. 5b) is then used as a 'representative' background concentration and subtracted from the detrended CO_2 time series. The final time series of CO_2 deviation is shown in Fig. 5c.

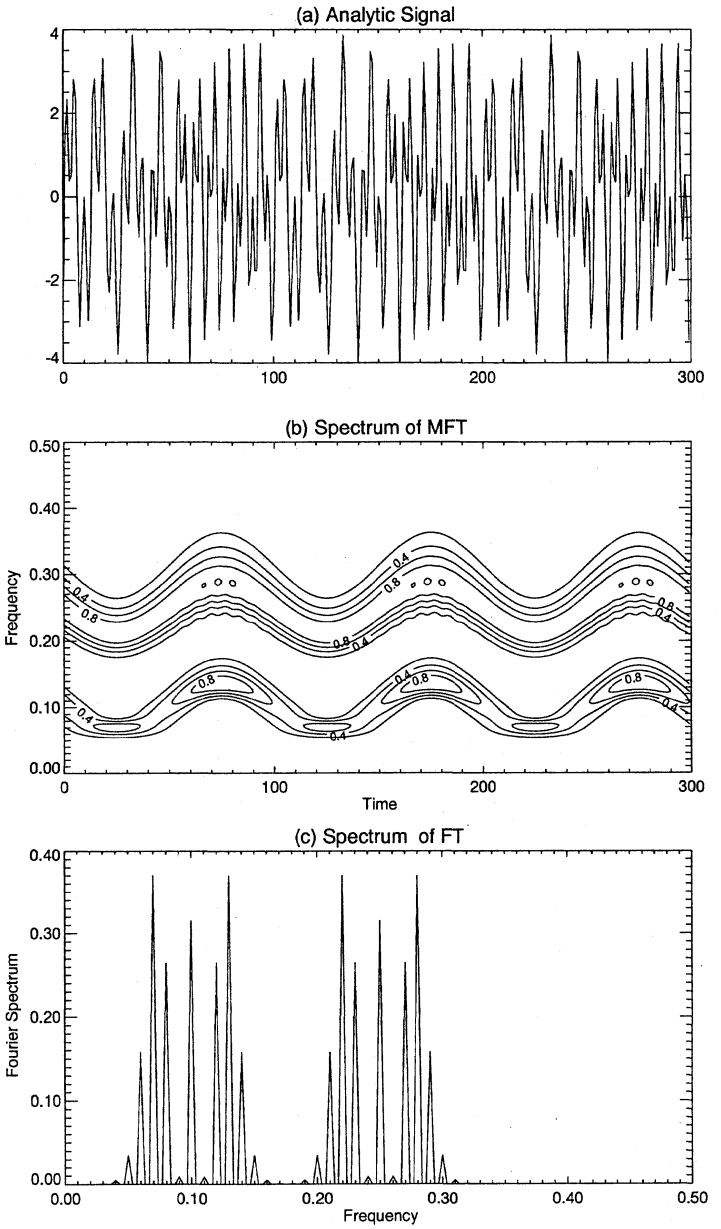

Fig. 3. MFT and FT analysis of frequency-modulated fluctuation: (a) time series; (b) spectrum of MFT (the contour interval is 0.2); (c) spectrum of FT.

Figure 6 shows the MFT spectra of the time series of CO_2 deviation in frequency and time domain. The short-term fluctuations occurring at different times and at different frequencies can be seen very clearly in this figure. Both the amplitude and the frequency of these fluctuations change with time, indicating their nonstationarity. Figure 6 also reveals that these CO_2 fluctuations are characterized by amplitude and frequency modulation, along the line discussed in the previous analytic section.

Figure 6 also shows that the CO_2 concentration over Alert has three dominant regimes of quasi-periodic fluctuation: 1) seasonal cycle, 2) 20–50 day intraseasonal fluctuation and 3) 6–14 day synoptic fluctuation. On the annual scale, the seasonal cycle is represented by a narrow horizontal bar near the bottom, which is a relatively weak signal since the composite average seasonal cycle has been removed prior to the MFT analysis. On the intraseasonal time scale, the principal fluctuation period varies with time, although the most pronounced fluctuation is in the 20–50 day range during the winter season. Both the amplitude and frequency are strongly modulated by the seasonal cycle. On the synoptic time scale, a most noticeable feature is the appearance of singularities which are displayed in the spectral plane of MFT as vertical streaks covering a wide range of frequencies. For instance, fluctuations in different frequency bands in a wide frequency range are nearly in phase during the 1992 and 1994 win-

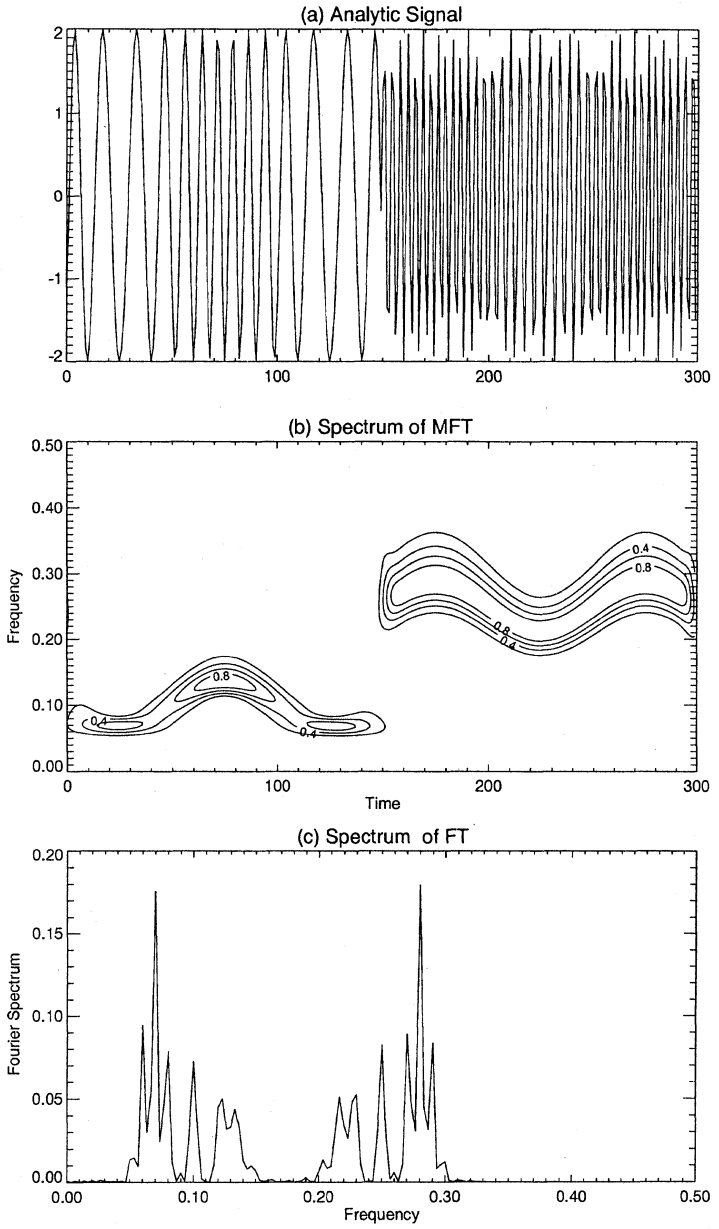

Fig. 4. MFT and FT analysis of the frequency-modulated fluctuation associated with abrupt change in frequency: (a) time series; (b) spectrum of MFT (the contour interval is 0.2); (c) spectrum of FT.

ters. In a similar manner to the intraseasonal fluctuations, these synoptic fluctuations are also strongly modulated by seasonal cycle, especially its amplitude.

To provide a better qualitative description of the interannual variability of the short-term fluctuations, seven segments of Fig. 6 and their average are displayed in Fig. 7. Each segment starts from 1 April of the first year and ends at 31 March of the next year. Even though there is a great deal of variability in the spectral signature from year to year, a certain pattern is apparent. The 7-year average (upper-left panel), for example, exhibits three peaks at periods corresponding to the seasonal cycle, 20–50 days and 6–14 days. The seasonal cycle is represented by the narrow color bar stretching across each segment at the bottom. This is slightly stronger during 88–89. The intraseasonal fluctuations of 20–50 days mainly occur during the winter season (November to February) and its dominant frequency shifts from about 0.04 (20 days) in early November to about 0.02 (50 days) in January and February. This kind of frequency modulation can be detected in most of the individual years on the intraseasonal time scale, such as 88–89, 90–91 and 91–92. In addition, a minor 20-day peak is detected in summer during the years 90–91, 92–93 and 93–94, although this peak is obscured in the 7-year average. The 6–14 days spectral peak averaged over 7 years is a little stronger than that of the 20–50 days peak during winter season.

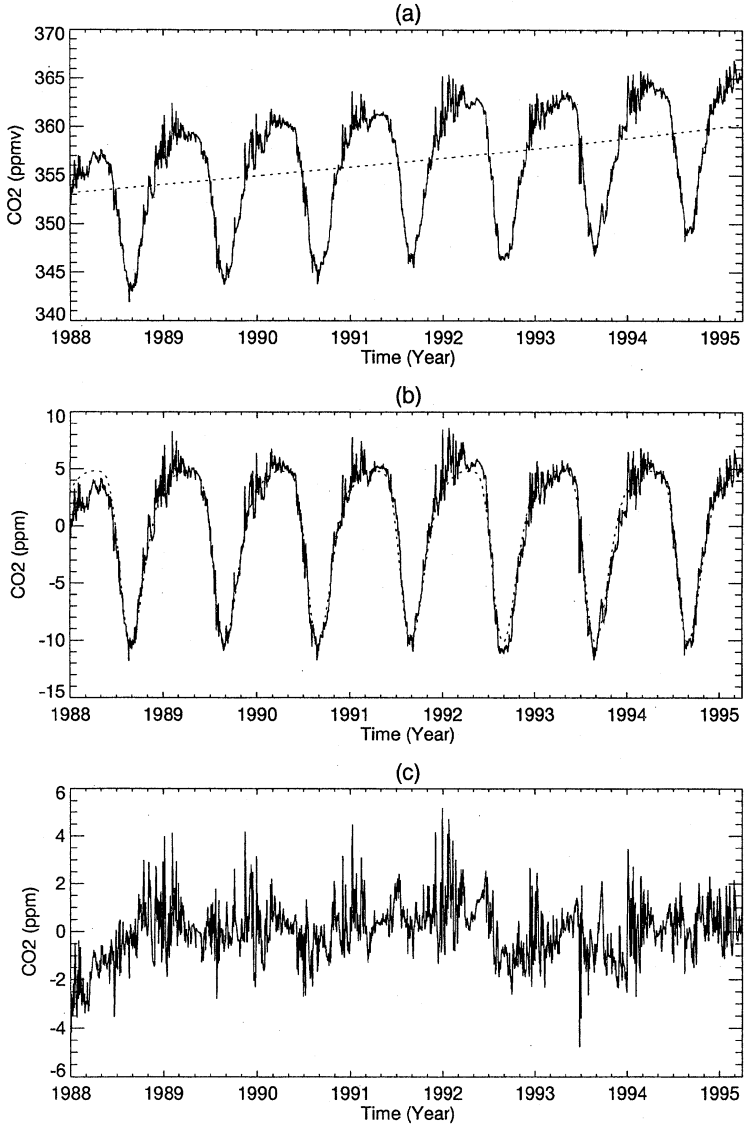

Fig. 5. CO_2 time series used in present study: (a) the original time series (solid line) and its long-term trend calculated by three-degree polynomial (dashed line); (b) the detrended time series (solid line) and its composite average seasonal cycle of CO_2 (dashed line); (c) the detrended and deseasonalised time series.

However, compared with the seasonal cycle and the intraseasonal fluctuations, the synoptic fluctuations of 6–14 days appear to show the strongest interannual variability. Figure 7 also shows a spectral peak in summer associated with periods from 6 to 14 days. The peak is quite evident during the summer of 89–90 and 93–94. The other two seasons, spring and fall, are quite quiescent.

From the amplitude and phase of MFT defined in Eqs. (24–27), we can define a sinusoidal function,

$$C(f,\tau) = A(f,\tau)cos[2\pi f\tau + \Phi(f,\tau)] \qquad (29)$$

which provides a combined depiction of amplitude and phase at a given frequency. The function, $C(f,\tau)$, evaluated at a particular frequency f, is called the "component". Figure 8 shows a breakdown of relative contributions made by some of the spectral components (periods= 6 days, 12 days, 20 days, 50 days,and 365 days) towards the variance of the detrended and deseasonalised CO_2 time series shown in Fig. 5c. Figures 8a–8d depict synoptic and intraseasonal fluctuations strongly modulated by the seasonal cycle, with the largest variability in these frequency ranges occurring generally in the winter season. Even though both the synoptic fluctuations (6–14 days) and the intraseasonal fluctuations (20–50 days) are strongly modulated by the seasonal cycle, the origins of these fluctuations are quite different. The synoptic fluctuations reflect the quasi-periodicity of the passage of synoptic systems (with different air masses) over Alert.

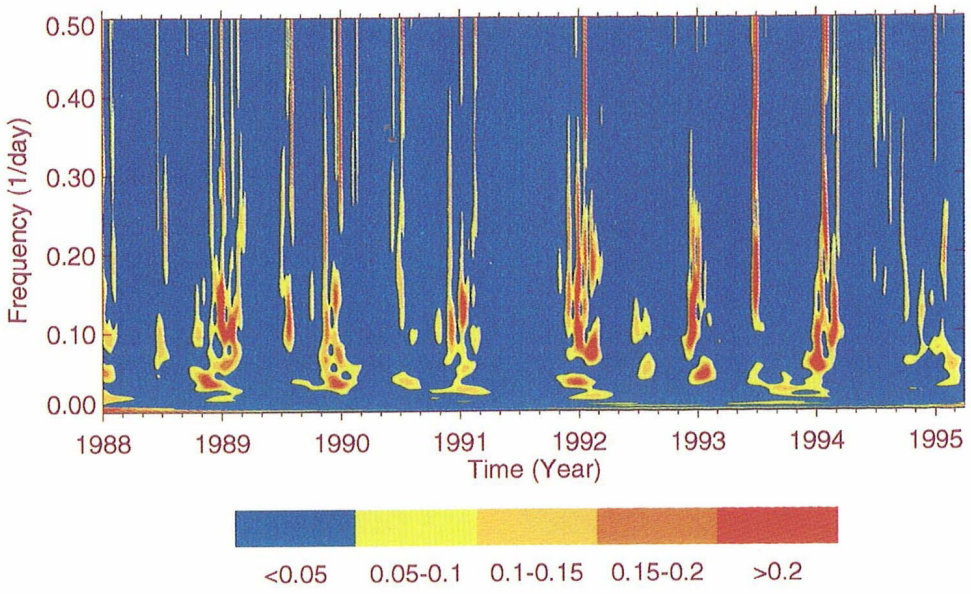

Fig. 6. MFT spectrum for CO_2 deviation. The abscissas are time (days) marching forward and the ordinates are frequency (*1/day*).

The low-frequency intraseasonal circulation variability of 20–50 days in the extratropics are discussed in such notable papers as Ghil and Mo (1991), Schubert and Park (1991), and the references quoted therein. These extratropical low-frequency oscillation modes appear to be associated with variability in the planetary wave structure, and seem to be well correlated with tropical convective activities in the tropics (Knutson and Weickmann, 1987). However, as Ghil and Mo (1991) have shown, the extratropical oscillation modes are often quite independent of what is happening in the tropical modes. Within the context of the present study, it is interesting to note that a reflection or impact of these low-frequency circulation modes can be detected in a CO_2 time series in the high Arctic.

Interannual variability in the amplitude of these components is also quite evident in Fig. 8. It is very likely that these synoptic to intraseasonal fluctuations, and their interannual variability, in the CO_2 measurements at Alert are caused by the variability in the atmospheric circulation and its transport processes (Yuen, *et al.*, 1996; Higuchi *et al.*, 1987; Higuchi and Daggupaty, 1985). The interannual variation in the annual cycle (period = 365 days) is shown in Fig. 8e. The range in the year-to-year variation of the amplitude of the CO_2 seasonal cycle at Alert appears to be around 0.4 ppmv. A large variation is detected in the years 1991 to 1993. The period, interestingly enough, corresponds to the time when the atmospheric CO_2 growth rate nearly went to zero globally. The large value at the beginning of the time series in Fig. 8e is less reliable than the rest of the record due to the endpoint effects.

As a comparison with the kind of information obtainable from a MFT analysis (Fig. 6), Fig. 9 shows a discrete Fourier spectrum of the 7-year CO_2 deviation time series shown in Fig. 5c. The result is basically a red spectrum with a peak around frequency 0.0025 (period = 400 days). Thus, the energy is concentrated mainly at the annual scale. Because of the nonstationary nature of the short-term fluctuations in the CO_2 measurements, there is no indication of the intraseasonal and synoptic variability in the Fourier spectral density.

6. Conclusions

In this paper we have attempted to provide a basic framework and some examples of an application of multiresolution Fourier transform (MFT) to CO_2 time series. The intention of this paper is to bring attention to this useful method for climate fluctuation analysis. In contrast to the usual Fourier transform analysis, which yields a time-mean spectrum, the MFT approach can reveal the temporal structure of a spectrum. This property of MFT is particularly valuable for investigating non-stationary fluctuations that exhibit locality in both frequency and time. The MFT method is designed to reveal scale characteristics in a signal. It provides a continuous view of the spectrum as a function of time and frequency.

To reveal the temporal structure of the CO_2 short-term fluctuations, we have applied MFT to display time-frequency characteristics of the CO_2 variation at Alert. The results show that the CO_2 concentration over Alert has two dominant régimes of quasi-periodic short-term fluctuations 1) 20–50-day

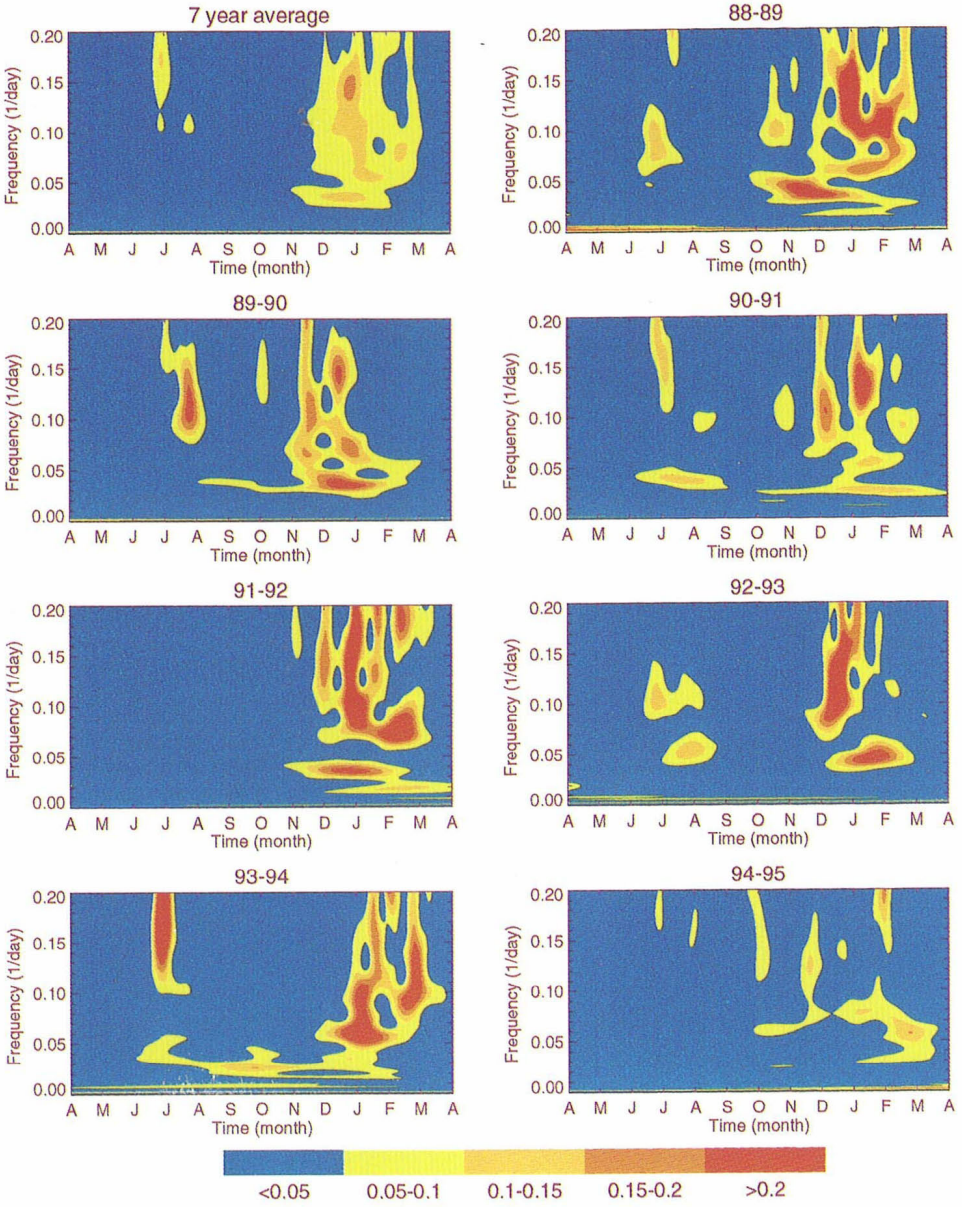

Fig. 7. MFT spectrum of CO_2 deviation for individual year (1988–1995) and its average over seven years.

intraseasonal fluctuation and 2) 6–14-day synoptic fluctuation. Both the amplitude and frequency of these fluctuations are strongly modulated by the seasonal cycle, with the largest amplitudes appearing during the winter season. In addition, these short-term fluctuations have significant interannual variability, especially for the synoptic fluctuation.

We speculate that the seasonally modulated short-term fluctuations revealed by the MFT analysis are related to atmospheric circulation variability (Peterson *et al.*, 1980; Perterson *et al.*, 1982; Halter and Peterson, 1981; Halter and Harris, 1983; Higuchi and Daggupaty, 1985; Higuchi *et al.*, 1987; Chung, 1988; Worthy *et al.*, 1994). Higuchi and Daggupaty (1985) and Higuchi *et al.* (1987) interpreted the variability of atmospheric CO_2 concentration at Alert, in terms of variation in the synoptic-scale atmospheric circulation.

The phase-locking relationship between the short-term fluctuations of CO_2 and the annual variation also suggests that northern ecosystems could constitute a large seasonally-dependent local CO_2 source. Indeed, a recent study has suggested that, although there is a large terrestrial carbon sink from 30–60°N, latitudes north of 60° may be a net CO_2 source (Ciais *et al.*, 1995). Some CO_2 measured at high latitudes is delivered from mid-latitudes by northward-moving winds (D'Arrigo *et al.*, 1987), but this cannot explain why maximum atmospheric concentrations occur at high latitudes. Northern ecosystems could constitute a large net source of CO_2, if their large pools of soil carbon are being released by soil

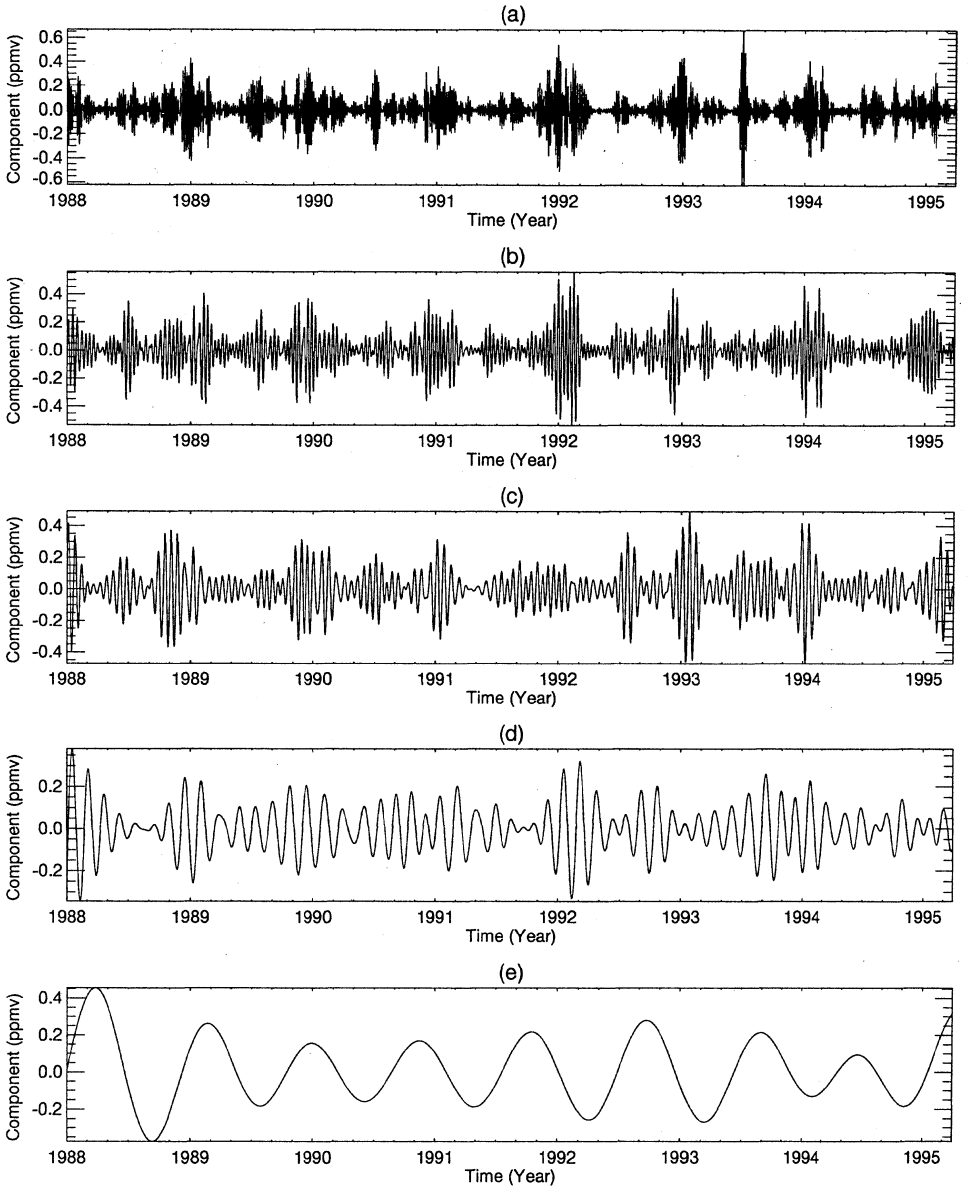

Fig. 8. The component of MFT at frequency (a) 1/6(day); (b) 1/12(day); (c) 1/20(day); (d) 1/50(day) and (e) 1/365(day).

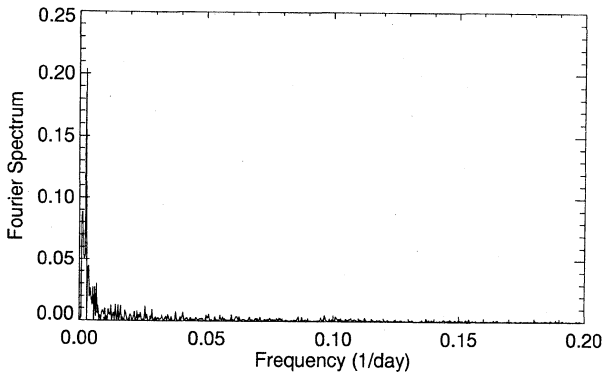

Fig. 9. Fourier spectrum for CO_2 deviation.

respiration, as suggested by recent measurements in Alaska (Oechel *et al.*, 1993) and Russia (Zimov *et al.*, 1996).

The present analysis revealed several important aspects of CO_2 variation over Alert, which require better physical understanding. Many additional analyses and numerical simulations need to be conducted in order to further understand the causes of fluctuation in atmospheric CO_2.

Acknowledgments

We would like to thank Drs. Christian Blanchette, Douglas Chan and Ken Yuen for useful discussions. Very useful comments by the two reviewers certainly have helped to improve the paper.

References

Chui, C.K., 1992: *An Introduction to Wavelets*, Academic Press.

Chung, Y.S., 1988: The variations of atmospheric carbon dioxide at Alert and Sable Island Canada. *Atmos. Environ.*, **22**, 383–394.

Ciais, P., P.P. Tans, M. Trolier, J.W.C. White and R.J. Francey, 1995: A large Northern Hemisphere terrestrial CO_2 sink indicated by the C^{13}/C^{12} ratio of atmospheric CO_2. *Nature*, **269**, 1098–1102.

Combes, J.M., A. Grossmann and Ph. Tchamitchian, editors, 1989: *Wavelets: Time-Frequency Methods and Phase Space*, Inverse problems and theoretical imaging, Springer-Verlag.

D'Arrigo, R., G.C. Jocoby and I.Y. Fung, 1987: Boreal forests and atmosphere-biosphere exchange of carbon dioxide. *Nature*, **329**, 321–323.

Daubechies, I., 1992: *Ten Lectures on Wavelets*, Number 61 in CBMS-NSF Series in Applied Mathematics. SIAM Publications, Philadelphia.

Engardt, M., K. Holmé and J. Heintzenberg, 1996: Short-term variation in atmospheric CO_2 at Ny-Alesund, Spitsbergen, during spring and summer. *Tellus*, **48B**, 33–43.

Foufoula-Georgiou, E. and P. Kumar, editors, 1994: *Wavelets in Geophysics*, Academic Press.

Gabor, D., 1946: Theory of communication. *J. IEEE* (London), **93**, 429–457.

Gamage, N. and W. Blumen, 1993: Comparative analysis of low-level cold fronts: wavelet, Fourier, and empirical orthogonal function decompositions. *Mon. Wea. Rev.*, **121**, 2867–2878.

Gambis, D., 1992: Wavelet transform analysis of the length of the day and the El Nino/Southern oscillation variations at intraseasonal and interannual time scales. *Ann. Geophys.*, **10**, 429–437.

Ghil, M. and K. Mo, 1991: Intraseasonal oscillations in the global atmosphere. Part I: northern hemisphere and tropics. *J. Atmos. Sci.*, **48**, 752–779.

Grossmann, A. and J. Morlet, 1984: Decomposition of Hardy functions into square integrable wavelets of constant shape, *SIAM J. Math. Anal.*, **15**, 723–736.

Gollmer, S., Harshvardhan, R.F. Cahalan and J.B. Snider, 1995: Windowed and wavelet analysis of marine stratocumulus cloud inhomogeneity. *J. Atmos. Sci.*, **52**, 3013–3030.

Halter, B.C. and J.M. Harris, 1983: On the variability of atmospheric carbon dioxide concentration at Barrow, Alaska, during winter. *J. Geophys. Res.*, **88** 6858–6864.

Halter, B.C. and J. Peterson, 1981: On the variability of atmospheric carbon dioxide concentration at Barrow, Alaska, during summer. *Atmos. Environ.*, **15**, 1391–1399.

Higuchi, K., V. Hudec, N.B.A. Trivett, D. Chan, C.W. Yuen and C.S. Wong, 1995: A statistical comparison of CO_2 measurements at Cape St. James and Station "P", Canada. *Tellus*, **47B**, 4–16.

Higuchi, K., N.B.A. Trivett and S.M. Daggupaty, 1987: A preliminary climatology of trajectories related to atmospheric CO_2 measurements at Alert and Mould Bay. *Atmos. Environ.* **21**, 1915–1926.

Higuchi, K. and S.M. Daggupaty, 1985: On variability of atmospheric carbon dioxide concentration at station Alert. *Atmos. Environ.* **19**, 2039–2044.

Huang, J.P. and G.R. North, 1996: Cyclic spectral analysis of fluctuation in a GCM simulation. *J. Atmos. Sci.*, **53**, 370–379.

Hudgins, L.H., C.A. Friehe and M.E. Mayer, 1993: Wavelet transforms and atmospheric turbulence. *Phys. Rev. Lett.*, November 15.

Hudgins, L.H. and J.P. Huang, 1996: Bivariate wavelet analysis of Asia monsoon and ENSO. *Advances in Atmospheric Sciences*, **13**, 299–312.

Knutson, T.R. and K.M. Weickmann, 1987: 30–60 day atmospheric oscillations: Composite life cycles of convection and circulation anomalies. *Mon. Wea. Rev.*, **115**, 1407–1436.

Lau, K.-M. and H.Y. Weng, 1995: Climate signal detection using wavelet transform: how to make a time series sing. *Bull. Amer. Meteor. Soc.*, **76**, 2391–2402.

Lejenäs, H. and K. Holmén, 1996: Characteristics of the large-scale circulation during episodes with high and low concentrations of carbon dioxide and air pollutant at an Arctic monitoring site in winter. *Atmos. Environ.* **17**, 3045–3057.

Mak, M., 1995: Orthogonal wavelet analysis: interannual variability in the surface temperature. *Bull. Amer. Meteor. Soc.*, **76**, 2391–2402.

Meyers, S.D., B.G. Kelley, and J.J. O'Brien, 1993: An introduction to wavelet analysis in oceanography and meteorology: with application to the dispersion of Yanai waves, *Mon. Wea. Rev.*, **121**, 2867–2878.

Oechel, W.C., S.J. Hastings, G. Vourlitis, M. Jenkins, G. Riechers and N. Grulke, 1993: Recent change of Arctic tundra ecosystems from a net carbon dioxide sink to a source, *Nature*, **361**, 520–523.

Pedlosky, J., 1970: Finite-amplitude baroclinic waves. *J. Atmos. Sci.*, **27**, 15–30.

Peterson, J.T., W.D. Komhyr, T.B. Harris and L.S. Waterman, 1982: Atmospheric carbon dioxide measurements at Barrow, Alaska, 1973–1979, *Tellus*, **34**, 166–175.

Peterson, J.T., K.J. Hanson, B.A. Bodhaine and S.J. Oltmans, 1980: Dependence of CO_2 , aerosol, and ozone concentrations on wind direction at Barrow, Alaska during winter. *Geophys. Res. Lett.*, **7**, 349–352.

Schubert, S.D. and C.-K. Park, 1991: Low-frequency intraseasonal tropical-extratropical interactions. *J. Atmos. Sci.*, **48**, 629–650.

Stockwell, R.G., L. Mansinha and R.P. Lowe, 1994: Location of the complex spectrum: the S transform. *AGU transactions*, **55**.

Trivett, N.B.A., K. Higuchi and S. Symington, 1989: Trends and seasonal cycles of atmospheric CO_2 over Alert, Sable Island, and Cape St. James, as analyzed by forward stepwise multiple regression technique. *The statistical Treatment of CO_2 Data Records.* ed. W. P. Elliott. NOAA technical Memorandum ERL ARL-173, Air Resources Laboratory, Silver Spring, Maryland, USA, 27–42.

Weng, H.Y. and K.-M. Lau, 1994: Wavelet, period-doubling and time-frequency localization with application to satellite data analysis. *J. Atmos. Sci.*, **51**,

2523–2541.
Wilson, R., A.D. Calway and E.R.S. Pearson, 1992: A generalized wavelet transform for Fourier analysis: the multiresolution Fourier transform and its application to image and audio signal analysis. *Info. Theory*, **38**, 674–690.
Worthy, D.E.J., N.B.A. Trivett, J.F. Hopper, J.W. Bottenheim and I. Levin, 1994: Analysis of long range transport events at Alert, N.W.T. during the Polar Sunrise Experiment. *J. Geophys. Res.* **99**, 25,329–25,344.
Yuen, C.W., K. Higuchi, N.B.A. Trivett and H.-R. Cho, 1996: A simulation of a large positive CO_2 anomaly over the Canadian Arctic Archipelago. *J. Meteor. Soc. Japan*, **74**, 781–795.
Zimov, S.A., S.P. Davidov, Y.V. Voropaev, S.F., Prosiannikov, I.P. Zimov, M.C. Chapin and F.S. Chapin, 1996: Siberian CO_2 efflux in winter as a CO_2 source and cause of seasonality in atmospheric CO_2. *Climatic Change*, **33**, 111–120.

多重解像度フーリエ解析と北極アラートにおけるCO_2濃度変動の解析への適用

Jian-Ping Huang・Kaz Higuchi・Neil B.A. Trivett
(Carbon Cycle Research Section, Atmospheric Environmental Service, Canada)

大気中のCO_2濃度の短周期変動を解釈するために、ウェーブレット理論を基にした多重解像度フーリエ解析(MFT)が利用できることを提案した。まず、幾つかの異なった合成信号を用いて検討した結果、時間と周波数において局在性を示す変動の解析にとって本解析は有用であると考えられた。

次に、MFTは1988年から1995年の間にアラートで観測されたCO_2濃度の変動を調べるために適用された。その結果、20–50日と6–14日の準周期的変動が顕著であり、これらの変動の振幅と周波数は季節変化によって強く変調され、また季節変化の最大振幅は冬期にみられることが見いだされた。さらに、これらの短周期変動(特に後者の変動)が明瞭な年々変動を示すことも明らかとなった。